Irreversibility and chaos in active particle suspensions

Sergio Chibbaro
Sorbonne Université, Centre National de la Recherche Scientifique, UMR 7190, Institut Jean Le Rond d'Alembert, F-75005 Paris, France

Astrid Decoene*
Université Paris Sud, Laboratoire de mathématiques d'Orsay (CNRS-UMR 8628), Bâtiment 425, 91405 Orsay cedex, France

Sebastien Martin
Université Paris Descartes, Laboratoire MAP5 (CNRS UMR 8145), 75270 Paris cedex 06, France

Fabien Vergnet
Université Paris Sud, Laboratoire de mathématiques d'Orsay (CNRS-UMR 8628), Bâtiment 425, 91405 Orsay cedex, France

(Received 7 June 2020; accepted 7 January 2021; published 26 January 2021)

We investigate the collective behavior of active suspensions of microswimmers immersed in a viscous fluid through numerical studies. We consider the two kind of organisms generally studied in experimental and theoretical studies, namely the *pullers* and the *pushers*, which differ in the way they are able to swim. We model them such that the body shape and the *flagella* used to swim are mathematical described. We tackle the problem using a new numerical approach, based on fictitious domains, which allows to fully solve the fluid-structure interaction and therefore exactly captures both the far- and near-field interactions between swimmers. Considering a two-dimensional domain for simplicity, we first investigate the state of bacterial turbulence in an unbounded domain, analyzing also their dynamical properties in terms of chaos. Then we analyze the rheological properties of the suspension by varying the different parameters. Our main findings are the following: (i) At variance with some previous studies, we show that pullers are able to trigger bacterial turbulence, although there is an asymmetry between ellipsoidal puller and pusher swimmers when elongated. (ii) Moreover, spherical pullers and pushers are found to be indistinguishable from a macroscopic point of view. (iii) We show that the complex dynamics, in particular the difference between pushers and pullers in collective properties, is related to a spontaneous breaking of the time-reversal symmetry. The key ingredients for breaking the symmetry are the concentration of the suspension and the shape of the organisms. (iv) The suspensions are chaotic in all cases, but that plays no role with regard to the macroscopic properties of the suspension. (v) Rheological signatures, already known in experiments, are analyzed and explained within this framework. We unambiguously show that our results are due to hydrodynamic interactions, whereas collisions or contacts do not play a role. The present results should be taken into account for the proposition of simplified models.

DOI: 10.1103/PhysRevFluids.6.013104

*astrid.decoene@math.orsay.fr

I. INTRODUCTION

Active matter undergoes intensive research for its relevance in medicine, ecology, and technological applications [1–5]. In nature, many living organisms swim through fluids at low Reynolds (Re) number [6], and a particularly interesting instance of such low-Reynolds number world is given by a suspension of self-propelled particles [7], which are essential in life cycle [8] as well as in bioengineering [9]. These microswimmers may exhibit complex dynamics as a result of the hydrodynamic interactions which stem from the swimming activity, unfolding large-scale motion characterized by a various phenomenology of patterns [10–16]. In particular, suspensions of bacteria at some concentration have been found to produce patterns of coherent motion sometimes called "bioturbulence", and under shear they yield the possibility to change the macroscopic viscosity of the suspending fluid viscosity [17–21]. An important experimental and theoretical activity has analyzed this problem, and notably previous analytical and numerical studies have shown that long-range correlations are a key ingredient to capture the main phenomenology [22–30], even though the precise mechanisms underlying the phenomenology remain to be fully understood [31–33].

These studies often deal with two kinds of flagellated swimmers, "pushers," such as *Bacillus subtilis* or *Escherichia coli*, which push themselves forward by using a flagellar apparatus localized at the back of the cell body, and "pullers" such as *Chlamydomonas reinhardtii*, which pull themselves forward through flagella attached at the front of their cell body that execute a breaststrokelike motion [21]. pushers are often modeled as dipolar swimmers exerting a force that expels fluid downstream, whereas pullers are modeled as dipolar swimmers acting in the opposite way. One of the most relevant observation of past theoretical studies is that bioturbulence appears to be triggered only by a suspension of *pushers*, whereas it is absent for *pullers* [30,34,35]. However, these theoretical or numerical studies make use of different levels of approximation either on the interactions or on the size of the objects, and notably the whole fluid-structure interaction has not yet been considered in dense suspensions without approximations, so that interactions cannot be said to be fully described.

In this work, we model the microswimmers taking into account the shape of the body and the distribution of the force, which is made along the flagella. We consider the presence of the fluid in the viscous approximation that leads to a Stokes problem for the hydrodynamics. Then, to solve the mathematical problem obtained, we present a new numerical approach that does not make use of any approximation other than considering a continuous medium, such that finite-size effects are taken into account together with the exact hydrodynamic interactions. The approach is based on a fictious-domain technique [36], which is similar and yet different from the immersed-boundary one [37]. We have developed an accurate method to handle possible contacts among particles.

The first purpose of the present work is to present extensive numerical simulations carried within this new approach to address the following issues: (i) Does bioturbulent state emerge both in suspensions of pushers and pullers or not as claimed in previous theoretical works? (ii) Which conditions are to be met to trigger such phenomenology? (iii) What are the mechanisms underlying such phenomena?

Since the organisms swim in a very viscous flow, a striking feature of these low-Reynolds-number flows is its reversibility in time [6,38]. The second aim of the work is to focus on this striking feature of microswimmers and to relate it to the observed collective behavior that appears at odd with it. More specifically, we shall investigate whether the difference in puller and pusher dynamics can be traced back to a spontaneous breaking of the hydrodynamics time-reversal symmetry and which are the mechanisms underlying such broken symmetry in biological swimmers. In order to comprehensively analyze this issue, we have investigated also the rheological properties, specifically the effective viscosity [21], of swimmer suspensions for both pullers and pushers at changing concentration, shape, and propulsion amplitude. As emphasized in statistical mechanics since Boltzmann [39–42], the relation between microscopic dynamics and macroscopic properties hides subtle issues, notably concerning the role of chaos and number of degrees of freedom [43–45]. In particular, it has been shown previously that non-Brownian passive suspensions break the

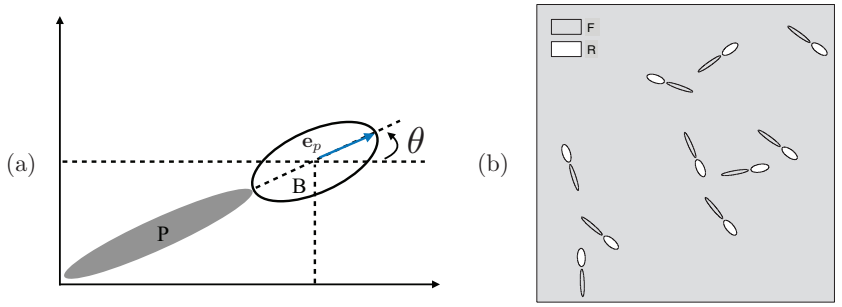

FIG. 1. (a) Schematic picture of the model for the pusher swimmer. (b) Domain Ω is made of a solid domain R (collection of rigid bodies of the bacteria) and a fluid domain $\Omega \setminus \bar{R} = F$.

time-reversal symmetry at the level of single particles, even though they are governed by reversible creeping equations [46]. The final purpose of our work is to address this issue for biological active matter, in particular looking at the chaotic properties of such suspensions, which has not been yet considered.

The paper is organized as follows: We present the theoretical framework, that is, the mathematical description of the bacterial suspension and the numerical approach used in Sec. II. Since the mathematical developments are complex, we provide some details in the Appendix. In Sec. III A, we show the results obtained for suspensions of pushers and pullers in an unbounded domain, that is, with periodic boundary conditions everywhere. The statistical observables analyzed include the root-mean-square velocity, the two-point or pair-correlation between swimmers. The main Lyapunov exponent (LE) is also displayed for several cases. In Sec. III B, we show the results concerning the rheological properties, notably the effective viscosity of the suspension at changing the different characteristics of the flow. The discussion is enriched by the analysis of the geometrical signatures of different suspensions and specifically the statistics of particle orientation. In the Conclusions, a summary and a general discussion of the results are drawn.

II. THEORETICAL FRAMEWORK

A. Physical model

We model each microorganism as a rigid ellipsoidal particle B immersed in the fluid, exerting a force $\mathbf{F}_P = -\kappa F \mathbf{e}_p$ on the fluid, homogeneously distributed inside a region denoted by P representing the flagellar bundle and an equal and opposite force $\mathbf{F}_B = \kappa F \mathbf{e}_p$ homogeneously distributed on the rigid body B; here $\mathbf{e}_p = (\cos\theta, \sin\theta)$ denotes the swimmer orientation, which is defined through the angle θ, as sketched in Fig. 1. The two types of swimmers are modeled in this way: In the case of pushers we take $\kappa = 1$ and in the case of pullers $\kappa = -1$, so that the flow field generated by one type of swimmer is the opposite of the other one. In the present model we do not consider random reorientation or tumbling [7,47] to focus on hydrodynamic effects.

A suspension of concentration ϕ is composed by N swimmers for the sake of simplicity in an open two-dimensional domain $\Omega =]0, L[^2$, filled with a Newtonian fluid. At the initial time the swimmers, denoted by $i = 1, \ldots, N$, are distributed randomly over the fluid (without overlapping). The position of the center of the ith particle is denoted by $\mathbf{x}_i$, and $\mathbf{v}_i$ and ω_i are its translational and angular velocities. The whole rigid domain is denoted by $R = \cup B_i$. The Reynolds number is typically less than 10^{-2} [48,49]; therefore inertial effects can be neglected and the fluid flow is described by the Stokes equations,

$$\begin{aligned} -\nabla \cdot \underline{\underline{\sigma}}(\mathbf{u}, p) &= \mathbf{f}_f \quad \text{in} \quad \Omega \setminus \bar{R}, \\ \nabla \cdot \mathbf{u} &= 0 \quad \text{in} \quad \Omega \setminus \bar{R}, \end{aligned} \tag{1}$$

where $\mathbf{u}$ and p are the velocity and pressure field in the fluid and where the stress tensor is $\underline{\underline{\sigma}} = 2\mu\mathbb{D}(\mathbf{u}) - p\,\mathbb{I}$, with $\mathbb{D}(\mathbf{u}) = \frac{\nabla\mathbf{u}+(\nabla\mathbf{u})^T}{2}$. Rigorously, the fluid equations are defined in the whole domain except in the closure of the rigid domain $\Omega \setminus \bar{R}$. The system is completed by specific boundary conditions: no-slip boundary conditions on the boundary ∂B_i of each rigid particle and periodic conditions on $\partial\Omega$, if not differently specified. The forces considered on the fluid are the forces exerted by the flagella:

$$\mathbf{f}_f = \sum_{i=1,\dots,N} \mathbf{F}_{P_i} \frac{\chi_{P_i}}{|P_i|},$$

where χ_{P_i} is the characteristic function associated to the region P_i and χ_{B_i} is the characteristic function associated to the particle B_i. Finally, force and torque balance for each body are written as follows:

$$\begin{aligned} \frac{1}{|B_i|}\int_{B_i} \mathbf{F}_{B_i} - \int_{\partial B_i} \underline{\underline{\sigma}} \cdot \mathbf{n} = 0 \quad \forall i \in \{1,\dots,N\}, \\ \int_{\partial B_i} (\mathbf{x} - \mathbf{x}_i) \times \underline{\underline{\sigma}} \cdot \mathbf{n} = 0 \quad \forall i \in \{1,\dots,N\}. \end{aligned} \tag{2}$$

The motion of each bacterium i is then set by its instantaneous velocity $\mathbf{u}(\mathbf{x}, t) = \mathbf{v}_i(t) + \omega_i(t) \times [\mathbf{x} - \mathbf{x}_i(t)]$ defined by ∂B_i, and the swimmers dynamics are set by the differential equations:

$$\dot{\mathbf{x}}_i(t) = \mathbf{v}_i(t)\,,\ \dot{\theta}_i(t) = \omega_i(t). \tag{3}$$

More precisely, the individual translational velocity is equal to the average velocity:

$$\mathbf{v}_i(t) = \frac{1}{|\partial B_i(t)|}\int_{\partial B_i} \mathbf{u}(t, \mathbf{x})\, d\mathbf{x}, \tag{4}$$

and the individual angular velocity is equal to

$$\omega_i(t) = \frac{1}{|\partial B_i(t)|} \frac{\int_{\partial B_i} \mathbf{u}(t, \mathbf{x}) \times [\mathbf{x} - \mathbf{x}_i(t)]\, d\mathbf{x}}{\int_{\partial B_i} |\mathbf{x} - \mathbf{x}_i(t)|^2\, d\mathbf{x}}. \tag{5}$$

The particles change their direction solely because of hydrodynamic interaction, since random reorientation is not present, and collisions are so rare that we can consider without compromise that they are absent, as explained also later.

It is important to stress here that Stokes equations do not contain the time, which enters the solution through boundary conditions because the configuration of the swimmers inside the fluid varies in time. That means that the time-reversal transformation $t \to -t$ and $\mathbf{V} \to -\mathbf{V}$ is equivalent to switch the puller dynamics into the pusher one and vice versa.

B. Numerical approach

The coupled fluid-particle problem (1) and (2) is solved using a finite-element method applied to solve the Stokes problem in the whole domain Ω and a penalty method to enforce the rigid motion constraint inside the rigid domain R. In order to prevent possible numerical overlap between rigid particles due to the numerical error, we use an approach proposed in Ref. [50] for spherical grains that we have extended to ellipsoidal particles in a viscous fluid. Denoting by $\Delta t > 0$ the time step, the time algorithm reads as follows: In a first step, the fluid-particle problem [Eqs. (1) and (2) in the main text] is solved without taking into account the possible overlapping of the particles (thus defining an *a priori* velocity of the swimmers), and then the projection of this *a priori* velocity onto a set of admissible velocities is computed. Finally, the position and orientation of each swimmer at time t^{n+1} are updated by solving the ODEs [Eq. (3) in the main text] using for instance a second-order Adam-Bashfort method. A more detailed description of this numerical strategy is given in the following.

1. A fictitious domain approach

The fictitious domain approach we use allows to avoid remeshing. We use a penalty method: The rigid motion constraint is obtained by relaxing a term in the variational formulation, which amounts to replacing rigid zones by highly viscous ones (see Refs. [51–53]). The mathematical problem is solved in the following constrained functional spaces:

$$K_\nabla \;=\; \big\{\mathbf{u} \in H_0^1(\Omega),\ \nabla\cdot\mathbf{u} = 0\big\}, \quad K_R \;=\; \big\{\mathbf{u} \in H_0^1(\Omega),\ \mathbb{D}(\mathbf{u}) = 0 \text{ a.e. in } R\big\}.$$

K_∇ is the space of divergence free functions defined on Ω and K_R is the space of functions which do not deform R. The solution to the initial problem, defined on $\Omega \setminus \bar{R}$, can be extended on the whole domain Ω by a function in K_R: $\mathbf{u}(\mathbf{x}, \cdot) = \mathbf{v}_i + \omega_i \times (\mathbf{x} - \mathbf{x}_i)$ in B_i for every i, and we still denote this extension by $\mathbf{u}$. The problem in variational form can then be written as the minimization of the functional

$$J(\mathbf{u}) \;=\; \mu \int_\Omega |\mathbb{D}(\mathbf{u})|^2 \;-\; \int_\Omega \mathbf{f}\cdot\mathbf{u}$$

on $K_R \cap K_\nabla$, where

$$\mathbf{f} = \sum_{i=1}^{N} \big(\mathbf{f}_b^i\, \chi_b^i + \mathbf{f}_p^i\, \chi_p^i\big).$$

The rigid motion constraint is relaxed by introducing the following penalty term in the functional to minimize:

$$\int_R \frac{1}{\varepsilon}\, \mathbb{D}(\mathbf{u}) \,:\, \mathbb{D}(\mathbf{u}),$$

so that $\mathbb{D}(\mathbf{u})$ goes to zero in R when ε goes to zero and $\mathbf{u}$ tends to a rigid motion in R. The variational formulation obtained is as follows: Find $\mathbf{u}_\epsilon \in H_0^1(\Omega)$ and $p \in L_0^2(\Omega)$ such that

$$2\mu \int_\Omega \mathbb{D}(\mathbf{u}_\epsilon) \,:\, \mathbb{D}(\widetilde{\mathbf{u}}) + \frac{2}{\varepsilon}\int_R \mathbb{D}(\mathbf{u}_\epsilon) \,:\, \mathbb{D}(\widetilde{\mathbf{u}}) - \int_\Omega p_\epsilon\, \nabla\cdot\widetilde{\mathbf{u}} = \int_\Omega \mathbf{f}\cdot\widetilde{\mathbf{u}}, \quad \forall \widetilde{\mathbf{u}} \in H_0^1(\Omega),$$
$$\int_\Omega q\, \nabla\cdot\mathbf{u}_\epsilon = 0, \quad \forall q \in L_0^2(\Omega), \tag{6}$$

It has been proven in Refs. [51,54] that the penalty method converges linearly in ε.

2. Contact algorithm

In the present hydrodynamic framework, it is known that contacts are not supposed to happen (see Refs. [55–57]). Yet in actual simulations, collisions between particles are likely to occur because of the numerical error. From a numerical point of view, it means that the particles may overlap when their positions are updated after the velocity field computation. The treatment of possible overlaps is crucial in the case of dense suspensions. To address this issue, we have extended to wet ellipses the numerical method already proposed for dry spheres [50]. The method consists of projecting the velocity field onto some convex admissible set depending on the current configuration, so that particles do not overlap. Note that this method is consistent in the sense that when the time and space steps tend to 0, no contacts occur. Since no analytical expression of the minimal distance between two ellipses is available, an approximation of this distance must be computed at each time by solving the problem of searching for the proximal points on each pair of ellipsoidal particles. In Appendix, we give some details about the algorithm used to handle the contacts.

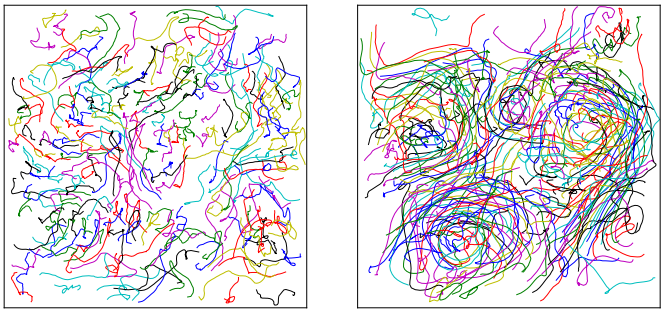

FIG. 2. Swimmer displacements or trajectories in the homogeneous biperiodic flow, after the transient period and with a volume fraction of $\phi = 0.3$. The left panel corresponds to elongated pullers, while the right one to elongated pushers.

III. RESULTS

A. Bioturbulence

In Fig. 2 several trajectories obtained by the simulation of pushers and pullers with elongated ellipsoidal shape are displayed. The dynamics is highly nontrivial in both cases, which highlights the nonlinear interaction among particles. Swimmers appear to form local inhomogeneities and to some extent synchronize their time trajectories, as found also in stochastic models [58,59]. Yet the two configurations show a significant difference in the collective motion: Pushers are able to build large rolls, as found also experimentally [13], while pullers appear to be coherent on a smaller time- and length scale but are nonetheless able to form collective rolls, as shown in the supplemental movie. It is worth emphasizing here that these results are purely a hydrodynamic effect, since we have used a such small time step where almost no collision is present.

To analyze quantitatively this issue, we have computed the root-mean-square velocity of the organisms as displayed in Fig. 3(a). In dilute suspensions, which are considered by definition those where no particle interaction is present, swimmers are basically isolated and the dynamics is the same for all species. Then the collective flow speed is highly increased by hydrodynamic interactions in moderate to dense suspensions for both swimmers. Remarkably, no difference is found for spherical objects, whereas pushers are found to create stronger collective velocity than

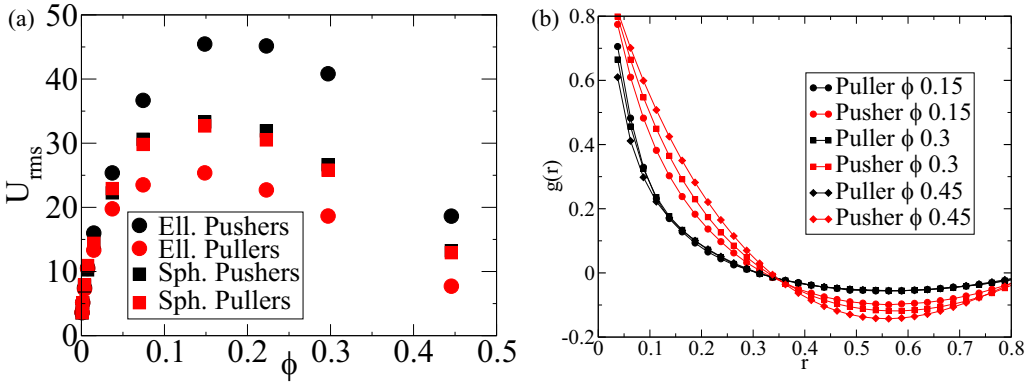

FIG. 3. (a) The root-mean-square velocity is defined as $U_{\rm rms} \equiv \sqrt{\langle U^2 \rangle_{p,t}}$. The average is computed both over all particles and in time. The velocity of the single particle is such that $U_{\rm rms} \approx 1$. (b) Two-point particle correlation computed for active ellipsoidal particles. Pushers are in red and pullers in black.

pullers when elongated shape is taken into account and the solid fraction is higher than few percentages. The increase in collective motion is of about one order of magnitude consistently with experimental observations [18]. The difference reaches a maximum at a concentration of around 20% and then decreases at higher concentration due to congestion in dense suspensions, resulting in the close-pack structural configuration of the rigid microswimmers [13]. Moreover, the mean velocity of the spheres is situated between ellipsoidal pushers and pullers.

In Fig. 3(b) we show the pair correlation of the particles, which is the order parameter that measures the level of coherent directional motion of the velocity field [13]. The field is defined as

$$g(r) = \left\langle \frac{\mathbf{v}(\mathbf{x}, t) \cdot \mathbf{v}(\mathbf{x} + \mathbf{r}, t)}{|\mathbf{v}(\mathbf{x}, t)||\mathbf{v}(\mathbf{x} + \mathbf{r}, t)|} \right\rangle_{p,t}, \tag{7}$$

where $\langle\rangle_{p,t}$ indicates average over time and over all particles. The pair-correlation points to the local organization of the system and indicates that active particles are able to manifest a certain level of coherence up to a certain integral length. The figure explains the qualitative picture discussed in the main text, as pushers shows a higher degree of organization up to a larger length, about $0.3L$, whereas pullers are less correlated and only on a smaller scale, about $0.2L$. Provided hydrodynamic interactions are effective $\phi \gtrsim 0.15$, the effect of the concentration is not strong and quite negligible for the case of pullers. In all cases some alignement is found, showing that pullers are also responsible for structures even though less coherent. The quantitative difference is traced back to the more or less aligned particles arising naturally from collective interactions, in accordance with experiments [13].

We note here that, as illustrated by the equations of motion, time dynamics is present in the system because of particle motion, yet hydrodynamics is reversible in time in the Stokes regime [55]. Therefore, the individual dynamics is symmetrical under time reversal, that is, $t \to -t$ and $\mathbf{V} \to -\mathbf{V}$. That means that by definition puller dynamics is formally obtained when the pusher dynamics is time reversed. The found asymmetry between pullers and pushers suggests a spontaneous time-symmetry breaking due to collective behavior. To highlight the issue, we have made the following experiment: We start a simulation with a pusher suspension, and at time t_0 we reverse the dynamics with a round-off error of 10^{-16}. In principle, given that the system is reversible, it should retrace its steps. It turns out that ellipsoidal swimmers, after a small amount of time in which the dynamics is reversed within numerical errors, break the time symmetry and switch from the pushers dynamics to the pullers dynamics, as shown in the Fig. 4. Instead, for spherical active particles, the forward and backward time trajectory is practically indistinguishable, at least from a statistical point of view. It is worth noting that we have displayed in Fig. 4 the experiment made with pushers but that we obtain the same picture doing the same time-reversal experiment with pullers, consistently with the equations of motion (2) and (3).

The fact that the transition from one dynamics to the other is quite fast after time reversal, as well as the irregular motion displayed in Fig. 1, suggests that swimmers are sensitive to small changes in the initial conditions; that is, they are chaotic in the sense of a positive Maximum Lyapunov exponent (LE) [60,61]. Since in some cases the macroscopic irreversibility of suspensions has been related to chaos [46,62,63], we quantify this sensitivity computing the LE λ for the two species of bacteria for different concentrations for ellipsoidal and spherical shapes. The LE is computed from the Euclidean distance between two simulations labeled 1,0 as $\Delta(t) = \frac{1}{N}\sqrt{\sum_{i=1}^{N}(x_i^1 - x_i^0)^2 + (y_i^1 - y_i^0)^2}$. The initial difference between the two simulations is set $|\delta\mathbf{x}|(t = 0) = 10^{-10}$ on only one particle, and for chaotic systems, Δ grows exponentially as $|\delta\mathbf{x}| \exp(\lambda t)$. To obtain smoother curves we average Δ over 50 different initial perturbations. The case with $\phi \approx 0.005$ is made with $N = 3$ and is studied when the particles are put initially aside as in Refs. [64,65].

As shown in Table I, all the cases are chaotic, except in the dilute regime where particles do not interact (we have verified that in the low-density regime no collision is encountered in any of our simulations). We can deduce that shape does not play any role in chaos, as found also for passive

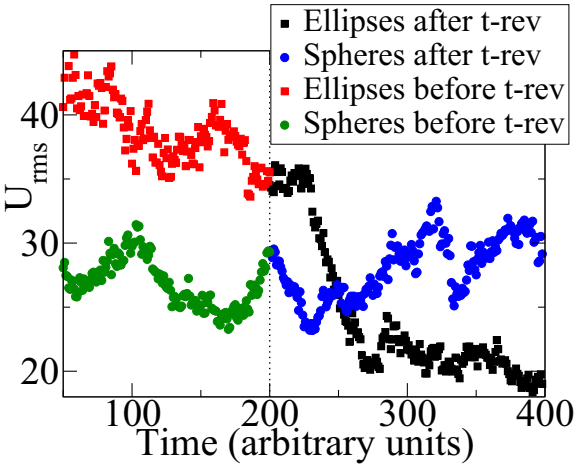

FIG. 4. Root-mean-square velocity averaged over all particles at each time step $U_{\rm rms} \equiv \sqrt{\langle U^2 \rangle_p}$ for the different kind of swimmers. Concentration is $\phi = 0.3$. At the time $t_0 = 200$ the dynamics is inverted, which means $t \to -t$ and $\mathbf{V} \to -\mathbf{V}$.

particles [46,62,64,65]. Indeed, for a given concentration we have not measured any difference neither changing shape neither between pullers and pushers. Instead, a dependence on ϕ is found: $\lambda \approx 0.1 \pm 0.01$ for $\phi \lesssim 0.2$ and $\lambda \approx 0.3 \pm 0.02$ for $\phi \gtrsim 0.2$.

Two mechanisms in principle can lead to such a chaotic behavior, the N-body hydrodynamical interactions and the short-range pair-contact ones. We have nevertheless verified that our results are insensitive to collisions, as already shown by the correct reversibility of spherical objects. Again, we have used a such fine discretization that particles do not reach each other except in very rare cases. Hence, long-range hydrodynamic interactions lead to a chaotic regime, which is responsible for the irreversibility at the level of the single particle trajectory, that is, at the microscopic level, as already observed for passive suspensions [46].

This property should not be called *stricto sensu* irreversibility, since irreversible phenomena concern macroscopic variables. Yet we have seen in Fig. 4 that the instantaneous root-mean-square velocity averaged over all particles is not perfectly symmetrical under time reversal also in the case of spheres. This interesting effect is due indeed to chaos. However, the time average of the statistics is stable and does not change, indicating that the microscopic effect is visible only for the relatively small amount of particles and disappears for macroscopic samples [42].

In summary, chaos does not play a role in the macroscopic irreversibility, that is, looking at the statistical characteristics emerging from the microscopic ones [66], and the macroscopic irreversibility is due to the large number of interacting particles together with the elongation. Chaos helps in the sense that because of the large propagation of the initial small error, the breaking of the

TABLE I. Lyapunov exponents for different concentrations and shapes.

ϕ	0.005	0.05	0.2
Pushers (ellips.)	0.11 ± 0.01	0.12 ± 0.01	0.28 ± 0.02
Pushers (spheres)	0.09 ± 0.01	0.1 ± 0.01	0.27 ± 0.02
Pullers (ellips.)	0.12 ± 0.01	0.12 ± 0.01	0.31 ± 0.02
Pullers (spheres)	0.1 ± 0.01	0.12 ± 0.01	0.29 ± 0.02

symmetry can be observed very rapidly. This result is analogous to what found for the irreversibility of gases [39,45] or in other models [43,67].

B. Rheological properties

We analyze now some of the rheological characteristics of swimmer suspensions.

The effective viscosity of a suspension of passive spherical particles in a fluid of viscosity μ depends on its volume fraction ϕ. In the dilute regime, where $\phi \ll 1$ so that particles do not interact, the effective viscosity is well described by Einstein's relation $\mu_{\text{eff}} \approx \mu_0(1+\alpha\phi)$, where α is known as Einstein's coefficient [68] and depends on the dimension and on the elongation of entities. The linear dependency with respect to volume fraction is due to the fact that, in this regime, the total effect of the particles on the viscosity is equal to the sum of individual contributions. Beyond the dilute regime, particles interact and thus simple addition of contributions is no more valid. Polynomial development of the form $\mu_{\text{eff}} \approx \mu_0(1+\alpha\phi+\beta\phi^2+\dots)$ is needed. Work in the semidilute regime, where interactions are moderate, has focused on finding coefficients for the higher-order terms in ϕ in a polynomial development of the form: $\mu_{\text{eff}} \approx \mu_0(1+\alpha\phi+\beta\phi^2+\dots)$. In the case of active suspensions, the measurement or computation of the effective viscosity is particularly interesting, since different phenomena can arise depending on the type of motion. It is well known that the viscosity of a suspension of particles is different from that of the solvent [69–71] and that shape of the particles has an effect [72]. Elongated pusherlike swimmers, for instance, tend to decrease the effective viscosity [73], while spherical ones have no rheological signature [74,75].

We focus on the study of the shear viscosity in a fluid confined between two parallel rigid plates with a steady relative shear motion. In this case one can measure the shear stress, which is defined as the average force applied by the fluid on the plates per surface unit in response to this shear $F = \int_\Gamma (\sigma \cdot \mathbf{n}) \cdot \boldsymbol{\tau}/(2L)$, where Γ denotes the surface of the two plates, L denotes the length of each plate, $\mathbf{n}$ is the normal vector Γ pointing outward, and $\boldsymbol{\tau}$ is the tangential vector on Γ opposed to the shear flow. For a suspension, an apparent viscosity is defined as $\mu_{\text{app}}(t) = F/\dot{\gamma}$, where $\dot{\gamma}$ denotes the shear rate. Since this value changes in time due to the evolution of the particle configuration, one usually considers the effective viscosity: $\mu_{\text{eff}} = \lim_{T\mapsto+\infty} 1/T \int_0^T \mu_{\text{app}}(t)\,dt$. We have computed the effective viscosity in suspensions of pusher- and pullerlike swimmers applying shear through nonhomogenous Dirichlet conditions at walls, while periodic boundary conditions are imposed on the left and right boundaries. We have considered concentrations up to little less than 45% volume fraction.

We analyze here the impact of the active (swimming) motion looking at the effective relative viscosity, that is, eliminating the rheological signature related to the passive suspension, see Fig. 5. Beyond the dilute regime, elongated pusherlike swimmers tend to decrease the effective viscosity, while pullers increase it. Yet spherical ones have no relative rheological signature, behaving like the passive ones. Furthermore, we found that puller and pushers act in a symmetrical way with respect to the corresponding spherical suspensions, as highlighted by Fig. 5. Our findings are in agreement with those obtained experimentally [21,73–75].

Our results show that three ingredients are needed in order for self-propelled swimmers to produce a rheological signature: propulsion, elongation, and hydrodynamic interactions. The explanation has been already given [21,73], and our numerical simulations naturally retrieve these mechanisms. A single active particle (pusher or puller) rotates with the same angular velocity as a passive particle of same shape, while performing an ellipsoidal trajectory with characteristics depending on its individual velocity and elongation. The contribution to apparent viscosity due to its activity depends on the orientation of the force dipole. The contribution of an active particle to apparent viscosity is maximal when the dipole of propulsion forces is against the flow, and it is minimal when this dipole helps the flow. But since the time spent by a particle in each orientation is symmetric with respect to the neutral position (when the dipole is oriented parallel to the walls and apparent viscosity is equal to the passive case), the contribution to viscosity due to the activity vanishes when averaging over one period. Thus we obtain the same effective viscosity as in the

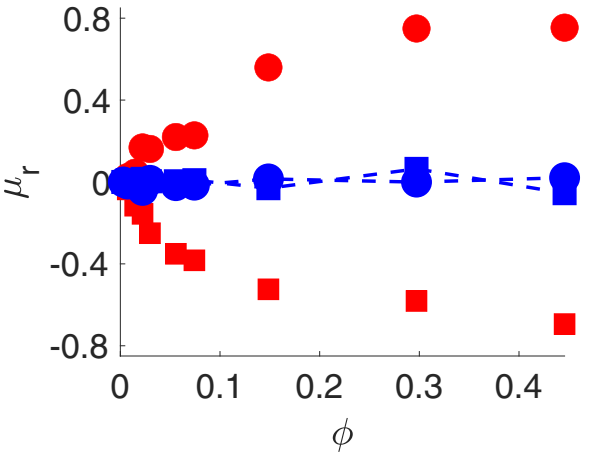

FIG. 5. Evolution with the concentration in a suspension of ellipsoidal pushers and pullers of the relative effective viscosity $\mu_r = (\mu - \mu_{\text{passive}})/\mu_{\text{passive}}$, where μ_{passive} is the effective viscosity of the suspension for nonactive particles. Pushers are indicated by the symbol □, and pullers by •. Red symbols indicate elongated particles, while blue-dashed ones are for spherical particles.

passive case. In the dilute regime, since effective viscosity is a result of the sum of contributions of each particle, self-propulsion has no impact on the rheology of the suspension. Beyond the dilute regime, hydrodynamic interactions disrupt the rotational behavior of individual swimmers. However, in the absence of a particular alignment of the active particles in the flow, the orientation of the population remains isotropic when averaging in time, and thus the effective viscosity remains the same as in the passive case. In the case of spherical active particles, there are no particular alignments and thus the activity of the particles has no impact on the effective viscosity. This is no longer true when the particles are elongated.

In order to quantitatively analyze this issue, we show in Fig. 6 the probability density function (pdf) of particle orientations obtained for the simulations with spherical and elongated particles in the passive and in the active cases. These results show again that if no other mechanism is added,

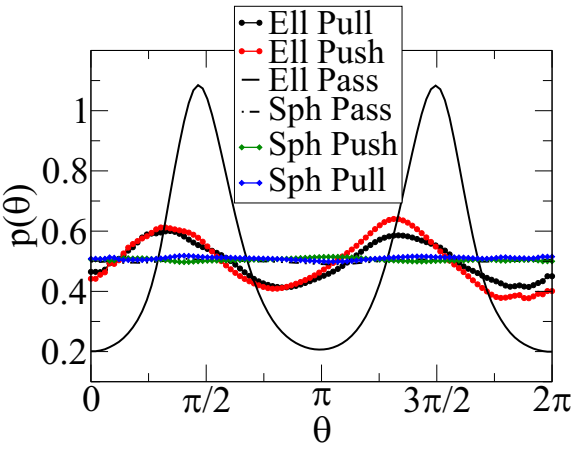

FIG. 6. Probability density function of particle orientations in the simulations of pusher, puller, and passive suspensions. The concentration is $\phi = 0.15$ and the ellipsoidal particles are of elongation ratio 2.

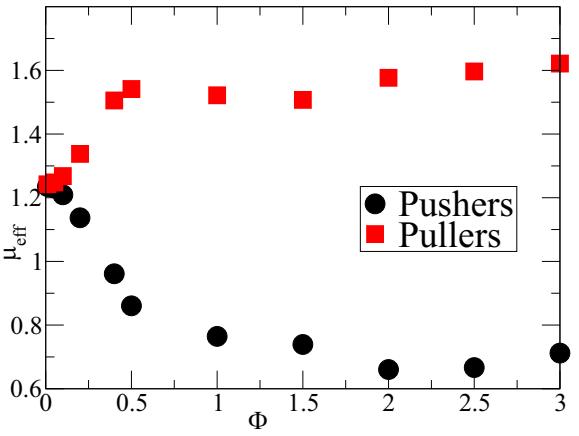

FIG. 7. Effective viscosity μ_{eff} with respect to Φ.

then elongation is needed to produce an additional rheological signature, which points out again the link to spontaneous symmetry breaking by shape. As displayed in Fig. 6, the symmetry with respect to the orientation is broken in the case of elongated particles. In fact, the latter tends to align in the flow at orientation $\pi/4$ (or equivalently $5\pi/4$), due to interactions with the other particles. Since active particles align in an orientation that maximizes apparent viscosity for pullerlike swimmers, and minimizes it for pusherlike swimmers, effective viscosity is enhanced in the first case and diminished in the second case. Spheres are not able to break the symmetry, and while they also align preferentially at two positions $\theta = \pi/2, 3\pi/2$, they stay the same amount of time at these two symmetrical positions, and rheological contribution hence averages to zero. Furthermore, our results show that steric interactions are not responsible for the collective properties of microswimmers.

As can be inferred from Fig. 6, the rheological features can be also understood through the spontaneous time-symmetry breaking by elongation, together with the activity. Indeed, this phenomenon is related to a preferential alignment in the flow at positions which maximize (minimize) the effective viscosity for active pullers (pushers). Yet passive ellipses have preferential alignments but symmetrical with respect to the neutral position and do not change the viscosity. Spheres are not able to break the symmetry and do not show any preferential alignment.

We have also investigated how the effective viscosity evolves when the ratio between activity of the microswimmers and shear rate changes, notably at varying the propulsion activity. For that purpose we introduce a nondimensional number that characterizes the shear flow in presence of microswimmers: $\Phi = \frac{f_p}{\mu S}$, where f_p is the magnitude of the propulsion force, μ is the viscosity of the fluid, and S the speed of the plates. As shown in Fig. 7, for low values of the propulsion-shear ratio, the effective viscosity in pusher (respectively, puller) suspensions decreases (respectively, increases) in a nonlinear way. But above a certain ratio, the effective viscosity stagnates, which is consistent with what found in the literature [19,21,73].

IV. CONCLUSIONS

We have reported on a numerical investigation of microswimmer suspension dynamics when organisms are immersed in a viscous fluid. In particular, we have studied two kind of bacteria, namely pushers and pullers as in main experimental and theoretical studies. The bacteria are modelled in such a way that shape and propulsion mechanism are in accordance with what is known from experiments. The corresponding mathematical problem constitutes a classical fluid-structure problem, where there is a mutual effect between particles and fluid. To solve this problem, we have proposed a new fictious-domain approach that allows for fully taking into account the fluid-structure

interaction, so that no approximation is made at the macroscopic level. It is important to stress here that we have verified in several ways that the contacts between particles are almost absent and in any case have no effect on the dynamics. That should represent a realistic picture of experimental conditions, where the density of particles does not reach the high critical limit at which steric interactions become comparable with lubrification forces [76,77]. While some of the phenomenology observed can be obtained with steric interaction based models [78,79], present results are therefore purely due to hydrodynamic interactions. We have not considered here the random reorientation called tumbling.

We have studied the pusher and puller dynamics at varying particle concentration in two main 2D configurations: (a) in unbounded domain where the free movement is able to generate a "bioturbulent" state and (b) in a flow sheared by two plates to study the rheological response of the suspension. Our numerical simulations are able to reproduce all the phenomenological features known for such kind of suspensions, notably the emergence of a macroscopic collective "turbulent" motion with an increase in the mean fluctuating energy of the flow, and an important change in the effective viscosity for ellipsoidal organisms.

The detailed numerical simulations have furthermore allowed to uncover the precise mechanisms and to bring new results:

(i) In order for nonlinear interactions among particles to be nonnegligible, a number of active particles large enough is needed. That triggers interactions between velocities, which induce chaotic motion of the particles, and their alignement, even without explicit interaction between directions. That leads to a kind of "bioturbulent" behavior with large-scale collective motion, for both pushers and pullers, at variance with what shown previously [24–27,34].

With regard to the chaotic properties, it is found that all the kind of suspensions are chaotic without important differences.

(ii) The presence of an elongated shape of the particles allows to spontaneously break the symmetry under time reversal which explains the impact of swimmers both on motion and rheology observed in the numerical experiments. As a consequence, spherical pullers are found to produce the same dynamics as spherical pushers, whereas ellipsoidal swimmers display a bioturbulent with different characteristics. In particular, pushers trigger a high-velocity motion.

We have therefore demonstrated that all the features displayed by our numerical experiments can be related to the spontaneous breaking of the time-reversal symmetry and that, as in the statistical mechanics of gases, while the number of agents is key, chaos does not play an important role. These results are relevant for the development of simplified models and artificial devices.

Concerning future developments, we plan to carry out fully 3D dynamical simulations via the present model and to compare directly with previous studies based on approximated theory. In particular, our analysis provides evidence that pullers are able to generate a turbulent state but lying on a different attractor from the pushers [80]. It would be interesting to quantify the degree of turbulence of both states to see to which extent they are different.

ACKNOWLEDGMENTS

We acknowledge useful discussions with Eric Clement, Hugues Chaté, and Bérengére Dubrulle. We thank Dr. Luca Caprini for the careful reading of the manuscript and his comments.

APPENDIX: CONTACTS

Let us detail the method in the case of spherical particles: We denote by $\mathbf{X}^n := (\mathbf{x}_i^n)_{i=1,\dots,N}$ the position of N particles (more precisely, the position of their gravity center) at time t_n and by $\hat{\mathbf{V}}^n$ their *a priori* velocity. We define the set

$$K(\mathbf{X}^n) = \{\mathbf{V} \in \mathbb{R}^{2N},\ D_{ij}(\mathbf{X}^n) + \Delta t\, \mathbf{G}_{ij}(\mathbf{X}^n) \cdot \mathbf{V} \geqslant 0,\ \forall i < j\}, \tag{A1}$$

where

$$D_{ij}(\mathbf{X}^n) = \left|\mathbf{x}_i^n - \mathbf{x}_j^n\right| - 2R_b$$

denotes the signed distance between two spheres B_i and B_j and

$$\mathbf{G}_{ij}(\mathbf{X}^n) = \nabla D_{ij}(\mathbf{X}^n) = \left(\ldots, 0, -\mathbf{e}_{ij}^n, 0, \ldots, 0, \mathbf{e}_{ij}^n, 0, \ldots\right), \quad \mathbf{e}_{ij}^n = \frac{\mathbf{x}_j^n - \mathbf{x}_i^n}{\left|\mathbf{x}_j^n - \mathbf{x}_i^n\right|}$$

is the gradient of the distance. In order to avoid overlapping, the following splitting procedure is proposed: In a first step, we solve the variational problem without taking into account the possible overlapping of the particles (thus defining an *a priori* velocity of the spheres) and then compute the projection of this *a priori* velocity onto the set of admissible velocities defined by (A1). The constrained problem is formulated as a saddle-point problem by using the introduction of Lagrange multipliers:

$$\begin{aligned} &\text{Find} \quad (\mathbf{V}^n, \boldsymbol{\Lambda}^n) \in \mathbb{R}^{2N} \times \mathbb{R}_+^{N(N-1)/2} \quad \text{such} \quad \text{that} \\ &\mathcal{J}(\mathbf{V}^n, \lambda) \leqslant \mathcal{J}(\mathbf{V}^n, \boldsymbol{\Lambda}^n) \leqslant \mathcal{J}(\mathbf{V}, \boldsymbol{\Lambda}^n), \quad \forall (\mathbf{V}, \lambda) \in \mathbb{R}^{2N} \times \mathbb{R}_+^{N(N-1)/2}, \end{aligned}$$

with the following functional:

$$\mathcal{J}(\mathbf{V}, \lambda) = \frac{1}{2}|\mathbf{V} - \hat{\mathbf{V}}^n|^2 - \sum_{1 \leqslant i < j \leqslant N} \lambda_{ij} \left(D_{ij}(\mathbf{X}^n) + \Delta t\, \mathbf{G}_{ij}(\mathbf{X}^n) \cdot \mathbf{V}\right).$$

Notice that the number of Lagrange multipliers corresponds to the number of possible contacts. In particular, if there is no contact between particles i and j, then $\Lambda_{ij} = 0$ and the Lagrange multiplier is not activated; conversely, if there is a contact between the two spheres, then Λ_{ij} may be positive and the corresponding auxiliary field allows the velocity field to satisfy the no-overlapping constraint. The approximate reaction fields $\boldsymbol{\Lambda}^n = (\Lambda_{ij}^n)$ is the dual component of a solution to the associated saddle-point problem. This problem is solved by an Uzawa algorithm (see, e.g., Ref. [81]).

In the case of ellipsoidal particles, the minimal distance between two ellipses is computed at each time by solving the problem of searching for the proximal points on a each pair of ellipsoidal particles. This problem can be defined in the following way: For all $i < j$, find $(\mathbf{x}_i, \mathbf{x}_j) \in \mathbb{R}^2$ such that

$$\mathbf{x}_i \in \partial B_i, \quad \mathbf{x}_j \in \partial B_j, \quad \mathbf{n}_i \cdot \mathbf{n}_j = -|n_i||n_j|, \quad \frac{\mathbf{n}_i}{|\mathbf{n}_i|} = \frac{\mathbf{x}_i\mathbf{x}_j}{\left|\mathbf{x}_i\mathbf{x}_j\right|},$$

where $\mathbf{n}_i$ and $\mathbf{n}_j$ are respectively the outward normal to ellipse B_i at point $\mathbf{x}_i$ and the outward normal to ellipse B_j at point $\mathbf{x}_j$. We use a Newton algorithm to numerically solve this problem. The method then consists of projecting the translational but also the angular velocity onto the set of admissible velocities associated to the current configuration.

[1] S. Ramaswamy, The mechanics and statistics of active matter, Ann. Rev. Condens. Matter Phys. **1**, 323 (2010).

[2] C. Bechinger, R. Di Leonardo, H. Löwen, C. Reichhardt, G. Volpe, and G. Volpe, Active particles in complex and crowded environments, Rev. Mod. Phys. **88**, 045006 (2016).

[3] D. L. Koch and G. Subramanian, Collective hydrodynamics of swimming microorganisms: living fluids, Annu. Rev. Fluid Mech. **43**, 637 (2011).

[4] M. C. Marchetti, J.-F. Joanny, S. Ramaswamy, T. B. Liverpool, J. Prost, M. Rao, and R. A. Simha, Hydrodynamics of soft active matter, Rev. Mod. Phys. **85**, 1143 (2013).

[5] E. Lauga, Bacterial hydrodynamics, Annu. Rev. Fluid Mech. **48**, 105 (2016).

[6] E. M. Purcell, Life at low reynolds number, Am. J. Phys. **45**, 3 (1977).
[7] T. J. Pedley and J. O. Kessler, Hydrodynamic phenomena in suspensions of swimming microorganisms, Annu. Rev. Fluid Mech. **24**, 313 (1992).
[8] W. H. Munk, Abyssal recipes, in *Deep Sea Research, and Oceanographic Abstracts*, Volume 13 (Elsevier, Amsterdam, 1966), pp. 707–730.
[9] R. Dreyfus, J. Baudry, M. L. Roper, M. Fermigier, H. A. Stone, and J. Bibette, Microscopic artificial swimmers, Nature **437**, 862 (2005).
[10] A. Sokolov and I. S. Aranson, Reduction of Viscosity in Suspension of Swimming Bacteria, Phys. Rev. Lett. **103**, 148101 (2009).
[11] S. Rafaï, L. Jibuti, and P. Peyla, Effective Viscosity of Microswimmer Suspensions, Phys. Rev. Lett. **104**, 098102 (2010).
[12] G. Mino, T. E. Mallouk, T. Darnige, M. Hoyos, J. Dauchet, J. Dunstan, R. Soto, Y. Wang, A. Rousselet, and E. Clement, Enhanced Diffusion Due to Active Swimmers at a Solid Surface, Phys. Rev. Lett. **106**, 048102 (2011).
[13] L. H. Cisneros, J. O. Kessler, S. Ganguly, and R. E. Goldstein, Dynamics of swimming bacteria: Transition to directional order at high concentration, Phys. Rev. E **83**, 061907 (2011).
[14] R. Rusconi, J. S. Guasto, and R. Stocker, Bacterial transport suppressed by fluid shear, Nat. Phys. **10**, 212 (2014).
[15] A. Kaiser, A. Peshkov, A. Sokolov, B. ten Hagen, H. Löwen, and I. S. Aranson, Transport Powered by Bacterial Turbulence, Phys. Rev. Lett. **112**, 158101 (2014).
[16] A. P. Petroff, X.-L. Wu, and A. Libchaber, Fast-Moving Bacteria Self-Organize into Active Two-Dimensional Crystals of Rotating Cells, Phys. Rev. Lett. **114**, 158102 (2015).
[17] C. Dombrowski, L. Cisneros, S. Chatkaew, R. E. Goldstein, and J. O. Kessler, Self-Concentration, and Large-Scale Coherence in Bacterial Dynamics, Phys. Rev. Lett. **93**, 098103 (2004).
[18] A. Sokolov, I. S. Aranson, J. O. Kessler, and R. E. Goldstein, Concentration Dependence of the Collective Dynamics of Swimming Bacteria, Phys. Rev. Lett. **98**, 158102 (2007).
[19] H. M. López, J. Gachelin, C. Douarche, H. Auradou, and E. Clément, Turning Bacteria Suspensions into Superfluids, Phys. Rev. Lett. **115**, 028301 (2015).
[20] V. A. Martinez, E. Clément, J. Arlt, C. Douarche, A. Dawson, J. Schwarz-Linek, A. K. Creppy, V. Škultéty, A. N. Morozov, H. Auradou *et al.*, A combined rheometry, and imaging study of viscosity reduction in bacterial suspensions, Proc. Natl. Acad. Sci. U.S.A. **117**, 2326 (2020).
[21] D. Saintillan, Rheology of active fluids, Annu. Rev. Fluid Mech. **50**, 563 (2018).
[22] K. Drescher, J. Dunkel, L. H. Cisneros, S. Ganguly, and R. E. Goldstein, Fluid dynamics, and noise in bacterial cell–cell, and cell–surface scattering, Proc. Natl. Acad. Sci. U.S.A. **108**, 10940 (2011).
[23] J. P. Hernandez-Ortiz, C. G. Stoltz, and M. D. Graham, Transport, and Collective Dynamics in Suspensions of Confined Swimming Particles, Phys. Rev. Lett. **95**, 204501 (2005).
[24] D. Saintillan and M. J. Shelley, Instabilities, and Pattern Formation in Active Particle Suspensions: Kinetic Theory, and Continuum Simulations, Phys. Rev. Lett. **100**, 178103 (2008).
[25] E. Lauga and T. R. Powers, The hydrodynamics of swimming microorganisms, Rep. Prog. Phys. **72**, 096601 (2009).
[26] D. Saintillan and M. J. Shelley, Emergence of coherent structures, and large-scale flows in motile suspensions, J. R. Soc., Interface **9**, 571 (2012).
[27] H. H. Wensink, J. Dunkel, S. Heidenreich, K. Drescher, R. E. Goldstein, H. Löwen, and J. M. Yeomans, Meso-scale turbulence in living fluids, Proc. Natl. Acad. Sci. U.S.A. **109**, 14308 (2012).
[28] J. Dunkel, S. Heidenreich, K. Drescher, H. H. Wensink, M. Bär, and R. E. Goldstein, Fluid Dynamics of Bacterial Turbulence, Phys. Rev. Lett. **110**, 228102 (2013).
[29] L. Jibuti, W. Zimmermann, S. Rafaï, and P. Peyla, Effective viscosity of a suspension of flagellar-beating microswimmers: Three-dimensional modeling, Phys. Rev. E **96**, 052610 (2017).
[30] D. Bárdfalvy, H. Nordanger, C. Nardini, A. Morozov, and J. Stenhammar, Particle-resolved lattice boltzmann simulations of 3-dimensional active turbulence, Soft Matter **15**, 7747 (2019).
[31] E. Sese-Sansa, I. Pagonabarraga, and D. Levis, Velocity alignment promotes motility-induced phase separation, Europhys. Lett. **124**, 30004 (2018).

[32] Y. Fily and M. C. Marchetti, Athermal Phase Separation of Self-Propelled Particles with no Alignment, Phys. Rev. Lett. **108**, 235702 (2012).
[33] L. Caprini, U. Marini Bettolo Marconi, and A. Puglisi, Spontaneous Velocity Alignment in Motility-Induced Phase Separation, Phys. Rev. Lett. **124**, 078001 (2020).
[34] J. Stenhammar, C. Nardini, R. W. Nash, D. Marenduzzo, and A. Morozov, Role of Correlations in the Collective Behavior of Microswimmer Suspensions, Phys. Rev. Lett. **119**, 028005 (2017).
[35] D. Bárdfalvy, S. Anjum, C. Nardini, A. Morozov, and J. Stenhammar, Symmetric mixtures of pusher, and puller microswimmers behave as noninteracting suspensions, Phys. Rev. Lett. **125**, 018003 (2020).
[36] P. Angot, C.-H. Bruneau, and P. Fabrie, A penalization method to take into account obstacles in incompressible viscous flows, Numer. Math. **81**, 497 (1999).
[37] C. S. Peskin, The immersed boundary method, Acta Num. **11**, 479 (2002).
[38] G. Taylor and J. Friedman, Low reynolds number flows (national committee for fluid mechanics films), 1966, https://techtv.mit.edu/collections/ifluids/videos/32604-low-reynolds-number-flow.
[39] C. Cercignani, *The Boltzmann Equation* (Springer, Berlin, 1988).
[40] L. Boltzmann, *Lectures on Gas Theory* (Courier Corporation, London, 2012).
[41] G. Gallavotti, *Nonequilibrium and Irreversibility* (Springer, Berlin, 2014).
[42] P. Castiglione, M. Falcioni, A. Lesne, and A. Vulpiani, *Chaos, and Coarse Graining in Statistical Mechanics* (Cambridge University Press, Cambridge, UK, 2008).
[43] J. Orban and A. Bellemans, Velocity-inversion, and irreversibility in a dilute gas of hard disks, Phys. Lett. A **24**, 620 (1967).
[44] J. L. Lebowitz, Boltzmann's entropy, and time's arrow, Phys. Today **46**, 32 (1993).
[45] S. Chibbaro, L. Rondoni, and A. Vulpiani, *Reductionism, Emergence, and Levels of Reality* (Springer, Berlin, 2014).
[46] D. J. Pine, J. P. Gollub, J. F. Brady, and A. M. Leshansky, Chaos, and threshold for irreversibility in sheared suspensions, Nature **438**, 997 (2005).
[47] B. M. Haines, A. Sokolov, I. S. Aranson, L. Berlyand, and D. A. Karpeev, Three-dimensional model for the effective viscosity of bacterial suspensions, Phys. Rev. E **80**, 041922 (2009).
[48] H. C. Berg, *Random Walks in Biology* (Princeton University Press, Princeton, NJ, 1983).
[49] C. A. Solari, J. O. Kessler, and R. E. Goldstein, Motility, mixing, and multicellularity, Genet. Progr. Evol. M. **8**, 115 (2007).
[50] B. Maury, A time-stepping scheme for inelastic collisions: Numerical handling of the nonoverlapping constraint, Numer. Math. **102**, 649 (2006).
[51] J. Janela, A. Lefebvre, and B. Maury, A penalty method for the simulation of fluid-rigid body interaction, ESAIM: Proc. **14**, 115 (2005).
[52] A. Lefebvre, Fluid-particle simulations with FreeFem++, ESAIM: Proc. **18**, 120 (2007).
[53] S. Vincent, J. P. Caltagirone, P. Lubin, and T. N. Randrianarivelo, An adaptative augmented Lagrangian method for three-dimensional multimaterial flows, Comput. Fluids **33**, 1273 (2004).
[54] B. Maury, Numerical analysis of a finite element/volume penalty method, SIAM J. Numer. Anal. **47**, 1126 (2009).
[55] C. K. Batchelor and G. K. Batchelor, *An Introduction to Fluid Dynamics* (Cambridge University Press, Cambridge, UK, 2000).
[56] D. Gérard-Varet and M. Hillairet, Regularity issues in the problem of fluid structure interaction, Arch. Ration. Mech. Anal. **195**, 375 (2010).
[57] M. Hillairet, Lack of collision between solid bodies in a 2D incompressible viscous flow, Comm. Part. Differ. Eq. **32**, 1345 (2007).
[58] B. ten Hagen, S. van Teeffelen, and H. Löwen, Brownian motion of a self-propelled particle, J. Phys.: Condens. Matter **23**, 194119 (2011).
[59] P. Romanczuk, M. Bär, W. Ebeling, B. Lindner, and L. Schimansky-Geier, Active brownian particles, Eur. Phys. J.: Spec. Top. **202**, 1 (2012).
[60] E. Ott, *Chaos in Dynamical Systems* (Cambridge University Press, Cambridge, UK, 2002).
[61] M. Cencini, F. Cecconi, and A. Vulpiani, *Chaos: From Simple Models to Complex Systems*, Series on Advances in Statistical Mechanics, Vol. 17, (World Scientific, Singapore, 2010).

[62] B. Metzger and J. E. Butler, Irreversibility, and chaos: Role of long-range hydrodynamic interactions in sheared suspensions, Phys. Rev. E **82**, 051406 (2010).
[63] B. Metzger, Phong Pham, and J. E. Butler, Irreversibility, and chaos: Role of lubrication interactions in sheared suspensions, Phys. Rev. E **87**, 052304 (2013).
[64] I. M. Jánosi, T. Tél, D. E. Wolf, and J. A. C. Gallas, Chaotic particle dynamics in viscous flows: The three-particle stokeslet problem, Phys. Rev. E **56**, 2858 (1997).
[65] G. Károlyi, Á. Péntek, I. Scheuring, T. Tél, and Z. Toroczkai, Chaotic flow: The physics of species coexistence, Proc. Natl. Acad. Sci. U.S.A. **97**, 13661 (2000).
[66] L. Landau and E. M. Lifshitz, *Course of Theoretical Physics: Statistical Physics*, Volume 5, (Pergamon Press, London, 2013).
[67] L. Cerino, F. Cecconi, M. Cencini, and A. Vulpiani, The role of the number of degrees of freedom, and chaos in macroscopic irreversibility, Physica A **442**, 486 (2016).
[68] M. Belzons, R. Blanc, J. L. Bouillot, and C Camoin, Viscosité d'une suspension diluée et bidimensionnelle de sphères, C. R. Acad. Sci., Paris II **292**, 939 (1981).
[69] A. Einstein, Eine neue bestimmung der molekldimensionen, Ann. Phys. **19**, 289 (1906).
[70] A. Einstein, Berichtigung zu meiner arbeit: Eine neue bestimmung der molekuldimensionen, Ann. Phys. **339**, 591 (1911).
[71] G. K. Batchelor, The effect of brownian motion on the bulk stress in a suspension of spherical particles, J. Fluid Mech. **83**, 97 (1977).
[72] H. Brenner, Rheology of a dilute suspension of axisymmetric brownian particles, Int. J. Multiphase Flow **1**, 195 (1974).
[73] V. Gyrya, K. Lipnikov, I. S. Aranson, and L. Berlyand, Effective shear viscosity, and dynamics of suspensions of micro-swimmers from small to moderate concentrations, J. Math. Biol. **62**, 707 (2011).
[74] B. M. Haines, I. S. Aranson, L. Berlyand, and D. A. Karpeev, Effective viscosity of dilute bacterial suspensions: a two-dimensional model, Phys. Biol. **5**, 046003 (2008).
[75] T. Ishikawa and T. J. Pedley, The rheology of a semi-dilute suspension of swimming model micro-organisms, J. Fluid Mech. **588**, 399 (10) 2007.
[76] E. Guazzelli and J. F. Morris, *A Physical Introduction to Suspension Dynamics*, Volume 45 (Cambridge University Press, Cambridge, UK, 2011).
[77] B. Andreotti, Y. Forterre, and O. Pouliquen, *Granular Media: Between Fluid, and Solid* (Cambridge University Press, Cambridge, UK, 2013).
[78] T. Vicsek, A. Czirók, Eshel Ben-Jacob, Inon Cohen, and O. Shochet, Novel Type of Phase Transition in a System of Self-Driven Particles, Phys. Rev. Lett. **75**, 1226 (1995).
[79] D. Nishiguchi, K. H. Nagai, H. Chaté, and M. Sano, Long-range nematic order, and anomalous fluctuations in suspensions of swimming filamentous bacteria, Phys. Rev. E **95**, 020601 (2017).
[80] G. Kawahara, M. Uhlmann, and L. V. Veen, The significance of simple invariant solutions in turbulent flows, Annu. Rev. Fluid Mech. **44**, 203 (2012).
[81] P. G. Ciarlet, *Introduction à l'analyse numérique matricielle et à l'optimisation* (Dunod, Malakoff Cedex, France, 1990).